REGULAR PAPER

Tae-Hyun Chang · Kwon-Soo Lee

An experimental study on swirling flow in a cylindrical annuli using the PIV technique

Abstract An experimental investigation was conducted to study the characteristics of turbulent swirling flow in an axisymmetric annuli. The swirl angle measurements were performed using a flow visualization technique using smoke and dye liquid for $Re = 60{,}000$–$80{,}000$. Using the two-dimensional particle image velocimetry method, this study found the time-mean velocity distribution and turbulent intensity in water with swirl for $Re = 20{,}000$, $30{,}000$, and $40{,}000$ along longitudinal sections. There were neutral points for equal axial velocity at $y/(R - r) = 0.7$–0.75, and the highest axial velocity was recorded near $y/(R - r) = 0.9$. Negative axial velocity was observed near the convex tube along $X/(D - d) = 3$–23.

List of symbols

D	Diameter of the concave tube (mm)
d	Diameter of the convex tube (mm)
L	Axial distance of the swirl chamber (mm)
R	Radius of the concave tube (mm)
r	Radius of the convex tube (mm)
Re	Reynolds number
U	Time averaged axial velocity (m/s)
u, v, w	Fluctuating velocity (m/s)
V	Time averaged radial velocity (m/s)
X	Axial coordinate of the test tube (mm)
y	Radial position from the wall (mm)
S	Swirl intensity $\left(S = 1/R \left[\int_0^r uwr^2 / \int_0^r u^2 r \, \mathrm{d}r \right] \right)$
θ	Swirl angle $\left(\theta = \tan^{-1} \frac{vw}{uv} \right)$

T.-H. Chang (✉)
RESEAT, Korea Institute of Science and Technology Information, Daejeon, Korea
E-mail: changtae@kyungnam.ac.kr

K.-S. Lee
Department of Mechanical and Automotive Engineering,
International University of Korea, san270 Sangmun-ri Munsan-eup,
Jinju, Kyungnam 660-759, Republic of Korea

1 Introduction

The flow in a cylindrical annuli, which has been widely utilized in boiler feed water heaters, heat exchangers between sea water and cooling water, tubular type heat exchangers, cyclotron and in cooling the rotor and stator of motors and generators, has been investigated extensively.

The initial investigation, by Rothfus (1948), sought to determine the friction coefficient and velocity profiles of the air flow in the tube, and in the 1949, sought to determine the turbulent intensity, and the Reynolds stress.

In 1964, using a Pitot tube and a hot wire anemometer, Brighton and Jones (1964) investigated the mean velocity, turbulent intensity, and Reynolds stress of water in the range of $Re = 46{,}000$–$327{,}000$.

Alan Quarmby (1967) measured the friction coefficient and velocity profile of water flow through the test tube for $Re = 6{,}000$–$9{,}000$, which had a ratio of $R/r = 2.88$–9.37.

Chigier and Beer (1964), Scott and Raske (1973), Milar (1979), Clayton and Morsi (1985) and Reddy et al. (1987) studied the swirling flow through a cylindrical annuli by measuring velocity profiles and pressure losses by applying the numerical analysis method. Recently, Chang and Kim (2001) measured various velocities and Reynolds stress profiles in the horizontal cylindrical tube using the particle image velocimetry method. However, investigations examining swirl flow are not enough to explain this kind of flow. Therefore, this study was performed in order to investigate the characteristics of swirl flow through visualization experiments of air flow, which is carried out using smoke and dye in the horizontal annuli of radius ratio.

$R/r = 3.0$ for $Re = 60{,}000$–$80{,}000$. The time-mean velocity and turbulence intensity of the swirling flow in an identical experimental rig were obtained using the two-dimensional particle image velocity method in water as the fluid for $Re = 20{,}000$–$40{,}000$. The present results will contribute to the economical design of heat exchangers.

2 Experimental apparatus

Figure 1 shows the layout of the experimental apparatus used in this study.

The experimental rig was manufactured from an acryl tube. A concave tube diameter of 150 mm and a length of 3,000 mm, a convex tube diameter of 50 mm and a length of 3,000 mm, and a stainless tube with an inner diameter of 50 mm and a length of 4,000 mm were used throughout this experiment. The swirl generator was installed at the entrance of the test tube. Because Taurus Controls Ltd certified their multi-pitot tube for the non-swirling flow but not for the swirling flow, a honeycomb was installed in the front of the test tube, and so it was possible for this tube to be use in the swirling flow.

The swirling generator was fabricated using an acryl tube with an outer diameter of 150.0 mm, in which eight holes with a diameter of 3.0 mm were drilled at 45° intervals from the outer to inner tangential direction. In order to adjust the swirling intensity, the swirling generator was designed to be able to move in the swirl chamber. Figure 2 represents a detailed diagram of the cross section of the swirl generator.

For the non-swirling flow experiment, the swirling generator and swirl chamber were dismantled and connected by a guide tube having the same diameter.
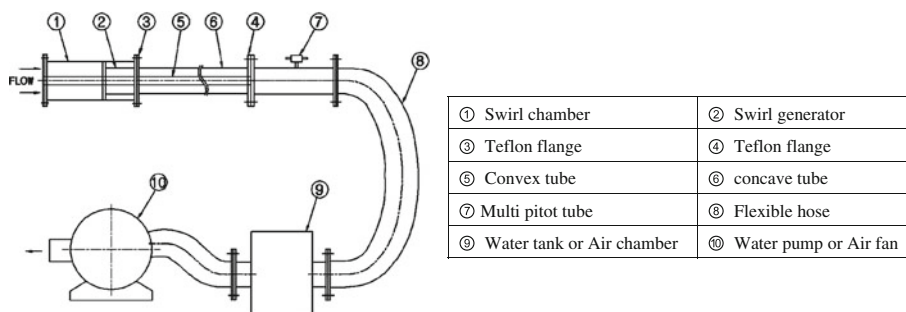

① Swirl chamber	② Swirl generator
③ Teflon flange	④ Teflon flange
⑤ Convex tube	⑥ concave tube
⑦ Multi pitot tube	⑧ Flexible hose
⑨ Water tank or Air chamber	⑩ Water pump or Air fan

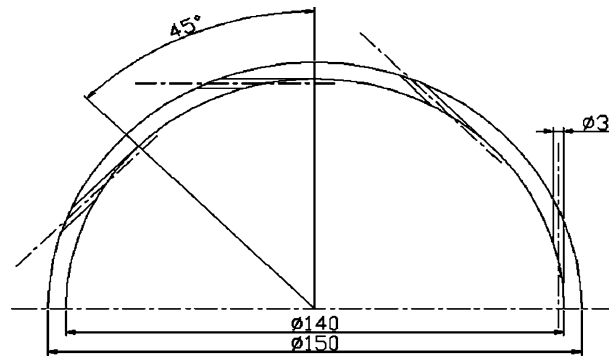**Fig. 1** Schematic diagram of the experimental apparatus

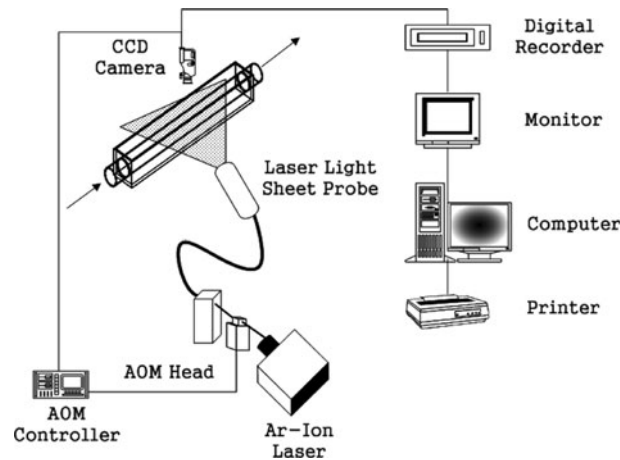**Fig. 2** Cross-section views through the swirl Generator

Fig. 3 Schematic arrangement of the PIV system

2.1 Experimental method and PIV system

In order to determine some of the swirl flow characteristics of the swirl flow induced by the swirl chamber used in this investigation, the flow visualization experiments were carried out first using smoke and dye liquid.

The velocities were measured using the 2D PIV technique, and the swirl motion of the fluid was produced by a tangential inlet condition. The algorithm used was the gray level cross-correlation method (Kimura et al. 1986). An Ar-ion laser was used and the light from the laser (500 mW) passes through a probe to make a two-dimensional light sheet. In order to make coded images of the tracer particles on one frame, an acoustic-optical modulator (AOM) was used. The AOM controller was synchronized with the camera and a carrier signal was sent to the AOM unit at 100 MHz, which enabled the AOM system to work as an electric shutter, as shown by Kobayashi et al. (1991).

The images taken through the camera were captured with a frame grabber (DT3155) and converted into 8-bit levels on the host computer. The particles used in the experiment were nylon 12 (50 μm). For these field images, the velocity vectors were obtained by using the PIV algorithm. The calculation time on the host computer (Pentium 550 MHz) was about 3 min in the case of the grid of 35×70, the radius for the searching area was set to 25 pixels, the size for the correlation area was set to 32×32 pixels. In order to eliminate erroneous vectors, an error vector elimination method based on the continuous flow condition was adopted.

In order to prohibit the refractive effects of the circular pipe on the results, a square box was installed, which recovered the refracted light waves from the visualized section of the flow. Figure 3 show the diagram of the PIV system used in this experiment.
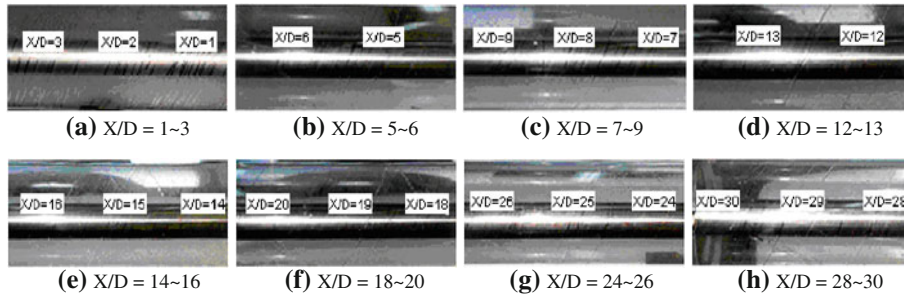
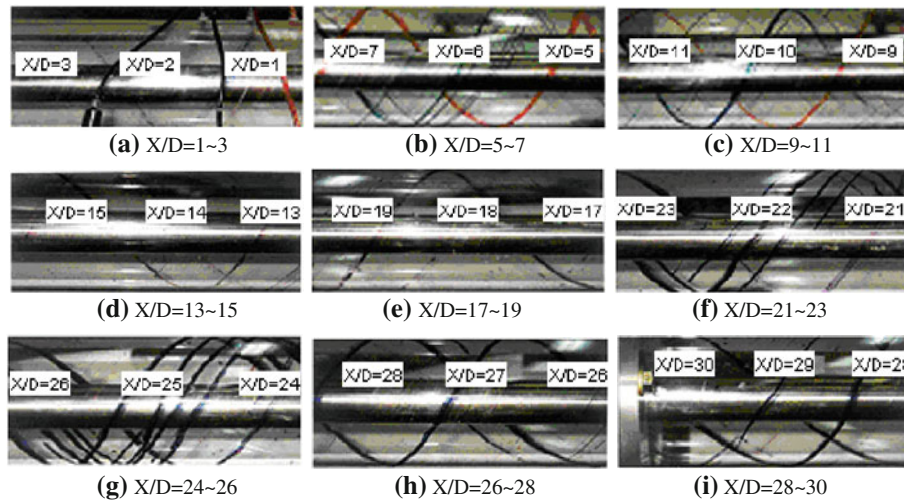**Fig. 4** Swirl angle distributions along the tube using smoke for $Re = 60,000$ at $L/D = 0$

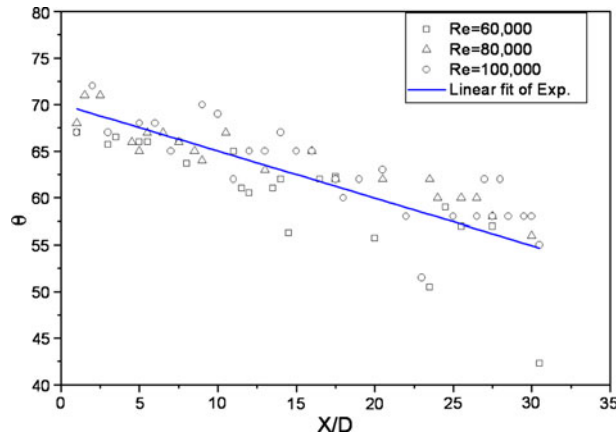**Fig. 5** Swirl angle distributions along the tube using dye liquid for $Re = 80,000$ at $L/D = 4$

Fig. 6 Comparisons of swirl angle for $Re = 60,000$, 80,000 and 100,000 at $L/D = 0$

3 Results and discussion

3.1 Swirl angle measurement

Several calculations have been performed based on experimental results in order to evaluate the swirl number and define the ratio of angular momentum to linear momentum flux. The 2D PIV technique is used

for velocity measurements. Therefore, in the present study, the Reynolds number rather than swirl number is used.

One of the primary objectives of this research was to measure the swirl flow angle along the test tube for different Reynolds numbers. The Reynolds number for these measurements ranged from 60,000 to 100,000 with $L/D = 0$–4.

During the flow visualization test, it was observed that some of the water-based liquid used to generate the smoke had condensed. This was deposited on the inside of the concave tube wall in the form of droplets that followed the path of the swirl flow.

Similar results were obtained by Sparrow and Chaboki (1984) who injected an oil lamp black mixture onto white plastic, self-adhering contact paper positioned inside the tube. By removing the paper, the angle made by the flow relative to the tube axis could be measured. In the present experiment, these angles were evaluated by placing a clear plastic sheet over the outside of the concave tube, tracing the streak lines, and then measuring the angle using a method similar to that of Sparrow and Chaboki (1984). The movement of
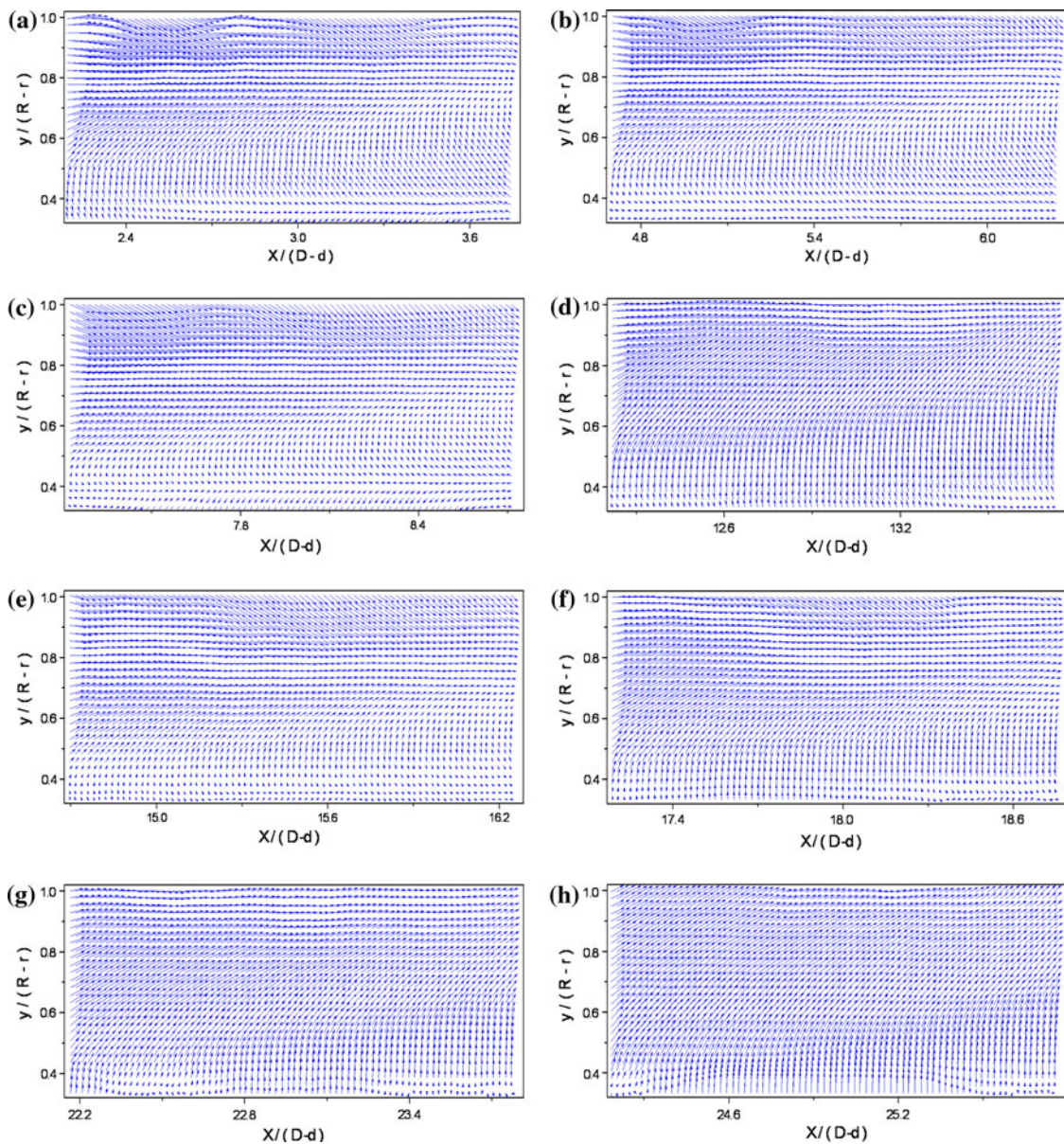

Fig. 7 Time-mean velocity vectors with swirl along the test tube for $Re = 20,000$ at **a** $X/(D − d) = 3.0$, **b** 5.5, **c** 8.0, **d** 13.0, **e** 15.5, **f** 18.0, **g** 23.0 and **h** 25.0

the droplets was, of course, due to the shear stress exerted by the flow at the tube wall. The flow angles were measured at eight pre-selected locations along the length of the test section tube.

The results obtained using smoke for $Re = 60,000$ are shown in Fig. 4. In each figure, flow angles are plotted as a function of X/D for both the extreme plenum chamber lengths ($L/D = 0$ and 4). Figure 5 shows the swirl angle using the dye liquid for $Re = 60,000$. Figure 6 illustrates the decay of the swirl angle along the test tube for $Re = 60,000–100,000$ and hence the ratio reduction of the tangential and axial shear stresses. The swirl flow starts with an angle of 70° with respect to the axial direction and decays to 55° at a location close to the end of the test section tube. This angle would have been zero in the case of a pure axial flow. Inspection of the figures shows that θ decreases with X/D, as shown earlier, and that increases in Reynolds number are accompanied by increases in the swirl angle θ.

At any fixed value of X/D and Reynolds number, the swirl angle increases as L/D is increased and as the swirl intensity is increased (i.e. $L/D = 0–4$).

The fitted θ versus X/D equations were of the form

$$\theta = 64.285 + \left(7.216 \times 10^{-5}\right) \times Re - 0.633 \frac{L}{D} - 0.504 \frac{X}{D} \tag{1}$$

This finding was further confirmed a lot of conditions with Reynolds number, X/D and L/D using smoke and dye liquid.

3.2 Velocity profiles

Figure 7 shows the time-mean velocity vector for $Re = 20,000$ along the test tube. The velocity vector was indicated as a negative value near the convex tube, and then the vector was changed to a positive vector after $X/(D-d) = 7$ with a decaying swirl intensity. However, a strong vector was observed near the concave tube, and in particular, uniform velocity vectors were observed at $y/(R-r) = 0.7–0.75$. The results appeared to be for a similar phenomenon that is not related to Reynolds number. In addition, these gradually disappeared along the test tube. These aspects were related to the decaying tangential velocity with swirl along the test tube. Figure 8 depicts the local axial velocities at $X/(D-d) = 3, 5.5, 8, 13, 15.5, 18, 23$ and 25 for $Re = 20,000$ that were calculated from the vector shown in Fig. 7.
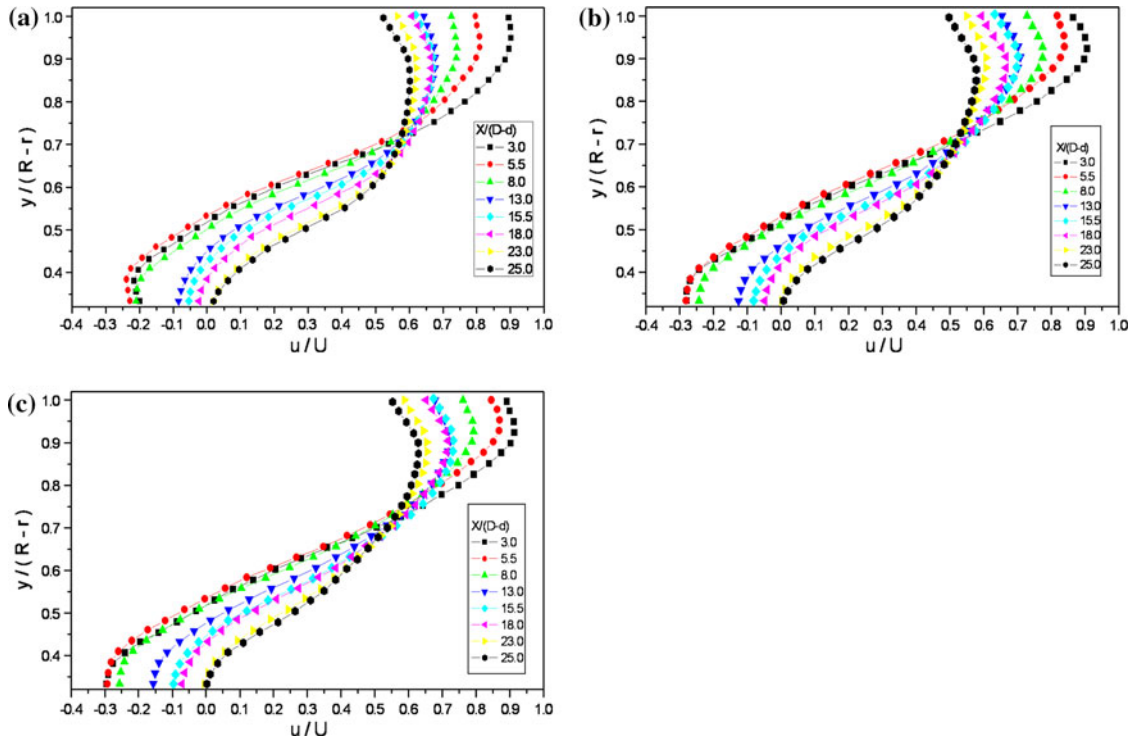

Fig. 8 Time-mean axial velocity profiles with swirl along the test tube for **a** $Re = 20,000$, **b** $Re = 30,000$ and **c** $Re = 40,000$

Figure 8 shows the local axial velocity profiles with swirl for $Re = 20,000$, 30,000 and 40,000. The local axial velocities in Fig. 8 show negative velocity profiles at $X/(D-d) = 3–25$ along the convex tube. The negative velocity region was increased according to increasing Reynolds number.

However, there is a neutral point for equal velocity at $y/(R-r) = 0.7–0.75$, and the highest velocity near $y/(R-r) = 0.9$. The maximum velocity point moved to the concave tube by increasing the Reynolds number, but the point also moved to the convex tube by the swirl flow decaying along the test tube.

Unlike in previous research on swirling flow, negative vectors and velocities were observed near the convex tube along $X/(D-d) = 3–25$. Phenomena such as these are similar to those associated with the swirling flow in a horizontal circular tube; however, the velocity gradient is smoother than that of a single tube with a swirl flow. Tangential velocity is thought to have quickly decayed through the concave and convex walls.

3.3 Turbulence intensity profiles

Figure 9 depicts the contours of axial turbulence intensity profiles calculated from the vectors for $Re = 20,000$. These intensities show maximum value near the concave wall and at $y/(R-r) = 0.5$. The former indicates the highest axial turbulence intensity near the concave wall as influenced by tangential velocity and the latter becomes associated with the boundary of the recirculating zone. These results were observed due to different velocity gradients existing next to each other near the convex wall. However, the
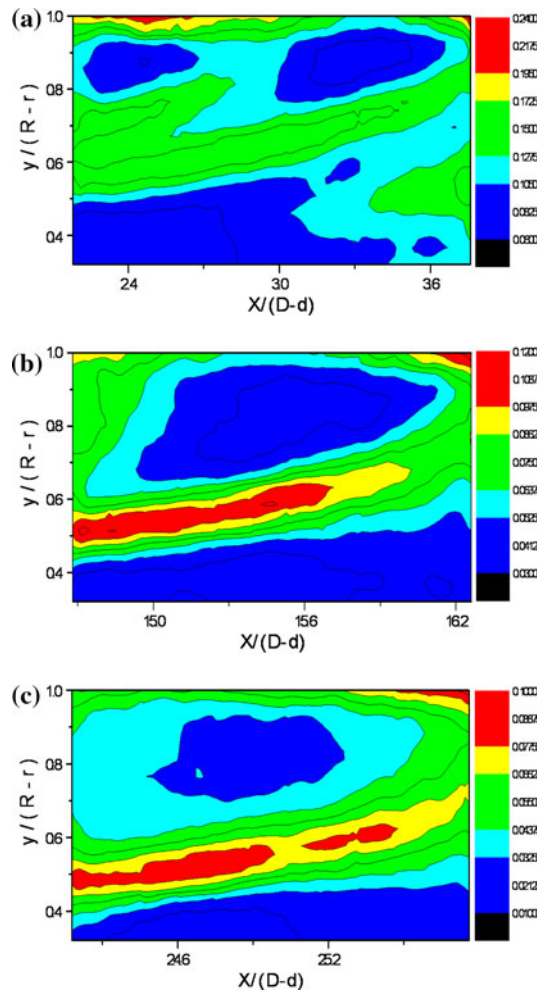

Fig. 9 Contours of axial turbulent intensity (u) along the test tube with swirl for $Re = 20,000$ at **a** $X/(D-d) = 3.0$, **b** 15.5 and **c** 25.0
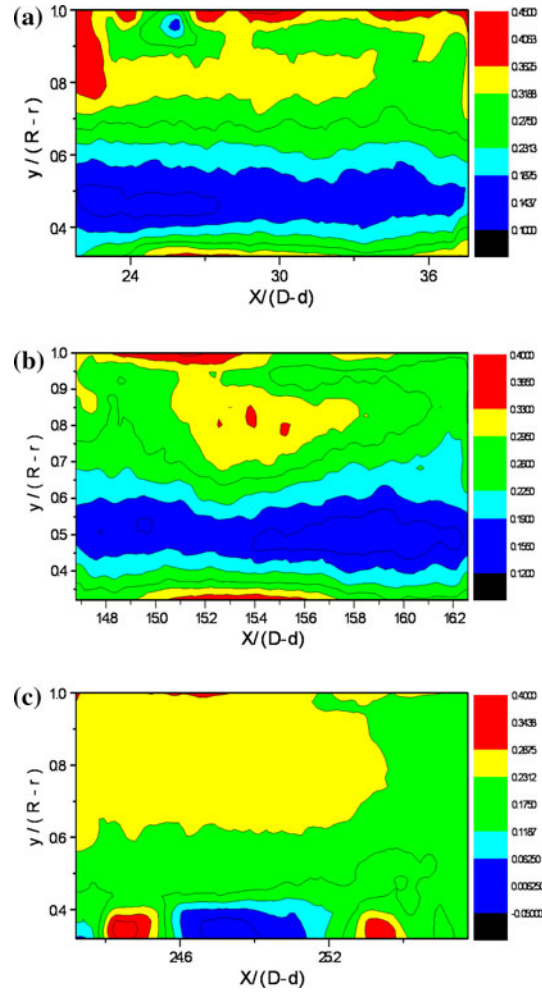
Fig. 10 Contours of radial turbulent intensity (v) along the test tube with swirl for $Re = 20{,}000$ along at **a** $X/(D - d) = 3.0$, **b** 15.5 and **c** 25.0

axial turbulence intensity was minimal at $y/(R - r) = 0.8$–0.9 and near the convex tube wall. This phenomenon was observed in association with the negative axial velocity.

The contour radial turbulence intensity profiles are plotted in Fig. 10. Unlike axial turbulence intensity, these intensities show strong values near the concave and convex tube walls. In addition, these intensities revealed an interesting phenomenon, the lowest radial turbulence intensity was observed near the boundary of the recirculating zone, $y/(R - r) = 0.5$. The results showed a similar phenomenon, although the Reynolds number continued to increase. This is thought to be associated with the strong swirl flow in the horizontal annuli.

4 Conclusions

The following conclusions were obtained for a cylindrical annuli by visualization and PIV techniques in air and water.

1. The swirl angle was derived from the following equation using a flow visualization test.

$$\theta = 64.285 + \left(7.216 \times 10^{-5}\right) \times Re - 0.633\frac{L}{D} - 0.504\frac{X}{D}$$

2. The velocity vector had a negative value near the convex tube and then the vector changed to a positive velocity after $X/(D - d) = 7$ with a decaying swirl intensity.

3. There were neutral points for equal axial velocity at $y/(R - r) = 0.7$–0.75, and the highest axial velocity was recorded near $y/(R - r) = 0.9$. Negative axial velocity was observed near the convex tube along $X/(D - d) = 3$–23.
4. The axial turbulence intensities showed maximum value near the concave wall and at $y/(R - r) = 0.5$. However, a particular phenomenon was observed when radial turbulence intensities were being investigated. The lowest intensity was noted near the boundary of the recirculating zone, $y/(R - r) = 0.5$.

References

Brighton JA, Jones JB (1964) Fully developed turbulent flow in annuli. J Basic Eng 86:835–844

Chang T, Kim H (2001) An investigation of swirling flow in a cylindrical tube. KSME Int J 15(12):1892–1899

Chigier AN, Beer JM (1964) Velocity and static-pressure distributions in swirling air jets issuing from annular and divergent nozzle. ASME J Basic Eng 86:788–796

Clayton BR, Morsi SM (1985) Determination of principal characteristics of turbulent swirling flow along annuli. Int J Heat Fluid Flow 6(1):31–41

Kimura I, Takamori T, Inoue T (1986) Image processing instrumentation of flow. Flow Vis 6(22):105–108

Kobayashi T, Saga T, Haeno T, Tsuda N (1991) Development of a real-time velocity measurement system for high reynolds fluid flow using a digital image processing design. In: Khalighia B et al. (eds) Experimental and numerical flow visualization ASME FED, vol 128, pp 9–14

Milar DA (1979) A calculation of laminar and turbulent swirling flows in a cylindrical annuli. ASME Winter Annual Meeting, New York, pp 89–98

Quarmby A (1967) An experimental study of turbulent flow through concentric annuli. Int J Mech Sci 9:205–221

Reddy PM, Kind RJ, Sjolander SAA (1987) Computation of turbulent swirling flow in an annular duct. Numerical methods in laminar and turbulent flow, pp 470–481

Rothfus RR (1948) Velocity distribution and fluid friction in concentric annuli. PhD thesis, Carnegie Institute of Technology

Scott CJ, Raske DR (1973) Turbulent viscosities for swirling flow in a stationary annulus. ASME J Fluid Eng 95:557–566

Sparrow EM, Chaboki A (1984) Swirl-affected turbulent fluid flow and heat in a circular tube. J Heat Transfer ASME 106:766–773